

# Closed loop image aided optimization for cold spray process based on molecular dynamics

Zhenxing Cheng<sup>a,b</sup>, Hu Wang<sup>a,\*</sup>, Gui-rong Liu<sup>b</sup>

<sup>a</sup>State Key Laboratory of Advanced Design and Manufacturing for Vehicle Body, Hunan University, Changsha, 410082, PR China

<sup>b</sup>Department of Aerospace Engineering and Engineering Mechanics, University of Cincinnati, Cincinnati, Ohio, 45221, United States

---

## Abstract

This study proposed a closed loop image aided optimization (CLIAO) method to improve the quality of deposition during the cold spray process. Some recent research shows that the quality of deposition measured by flattening ratio of the bonded particle is associated with impact velocity, angle and particle size. Therefore, the original idea of CLIAO is to improve the quality of deposition by obtaining the maximum flattening ratio which is extracted from the molecular dynamics (MD) simulation snapshots directly. To complete this strategy, a Python script is suggested to generate the required snapshots from result files automatically and the image processing technique is used to evaluate the flattening ratio from the snapshots. Moreover, three optimization methods including surrogate optimization (Efficient Global Optimization) and heuristic algorithms (Particle Swarm Optimization, Different Evolution algorithm) are engaged. Then a back propagation neural network (BPNN) is used to accelerate the process of optimization, where the BPNN is used to build the meta-model instead of the forward calculation. The optimization result demonstrates that all the above methods can obtain the acceptable solution. The comparison between those methods is also given and the selection of them should be determined by the trade-off between efficiency and accuracy.

*Keywords:* Molecular dynamic, Image processing technique, Optimization, Cold spray, Back propagation neural network

---

## Highlights

- A closed loop image aided optimization is suggested for the cold spray process;
- Several optimization methods are engaged including surrogate model and heuristic algorithms;
- An image processing technique is used to evaluate the objective function from the result contours directly;
- A back propagation neural network is constructed to accelerate the process of classic optimization methods.

## 1. Introduction

Cold spray is an innovative solid-state material deposition process, where micron sized particles bond to the substrate as a result of high-velocity impact. Compared with thermal spray, the powder remains in the solid state during the entire process which results in reduced oxidation and absence of phase transition.

---

\*Corresponding author

Email address: wanghu@hnu.edu.cn (Hu Wang)

Therefore, cold spray is widely used to temperature sensitive (such as nanostructured and amorphous) and oxygen sensitive (such as aluminum, copper, titanium, zinc, etc.) materials [1]. During the cold spray process, the particles are accelerated to the speeds between 300-1200 m/s by propellant gas and then impact on the substrate to form the plastic deformation and bonding connection which is shown in Figure 1. Cold spray was originally developed as a coating technology in the 1980s [2] and then became one of the most popular solid-state process due to its distinctive features in repairing turbine and compressor blades without changing their highly complex crystal structure [3]. Along the way, a number of academic studies on cold spray have been proposed which covering various aspects of the process and its applications [3–7]. Generally, those studies can be divided into two categories: mathematical modeling of impact using numerical methods and experimental investigations.

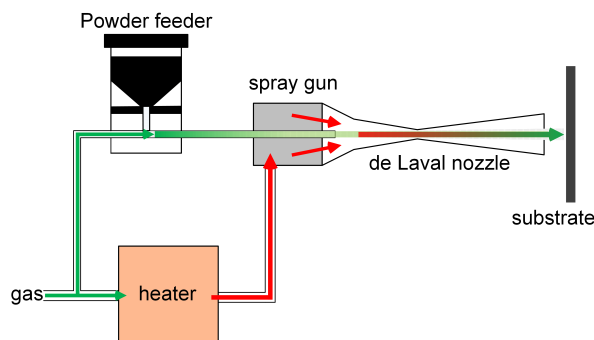


Figure 1: Schematic of Cold Spray Process [8].

As for the mathematical modeling, there are numerous studies on numerical simulation of cold spray process. Finite element method (FEM) is one of the wide-used numerical methods for cold spray and the finite element method software ABAQUS Explicit has been widely used to simulate the particle deformation [9–12], bonding features and associated mechanisms [13–15] in cold spraying. These studies are based on Lagrangian formulation. A general feature in Lagrangian-based FEM simulations is that they can demonstrate the interface between particle and substrate during the process of high speed impact, but it cannot reveal the realistic development of the deformation pattern due to the excessive mesh distortion. Nevertheless, the Eulerian-based FEM does not have such drawback, so it offers a more realistic account of the deformation geometry [4]. Then an Eulerian-based FEM software package named CTH, which was developed by Sandia National Laboratories, has been used to analyze the interfacing bonding in the cold spray process [16]. Furthermore, both Lagrangian and Eulerian FEMs are mesh-based methods. There have also been some attempts to simulate cold spray using mesh-free methods, such as smoothed particle hydrodynamics (SPH) and molecular dynamics (MD). SPH is a non-mesh-based numerical method that can avoid the problems associated with extreme mesh distortion. Studies of simulating cold spray using SPH include the work by Manap et al. [17] and Li et al. [18]. However, the process of bonding and rebounding is still cannot be demonstrated by neither FEM nor SPH method because the bonding happens at atom scale during the cold spray process. Therefore, MD method is considered as an ideal tool to simulate the bonding of cold spray but there are few studies focused on this. The earlier research is relevant to the aerosol deposition which revealed that higher impact velocities led to a stronger interface [19, 20]. Recently, some scholars and researchers have made progress in simulating cold spray process by MD method. For instance, Yao et al. have simulated collision behavior between nano-scale  $\text{TiO}_2$  particles during cold spray [21] and Joshi et al. modeled the whole cold spray process in nanometer dimension [22]. These studies investigated the bonding mechanism in cold spray process and understood the effect of critical parameters including impact velocity, angle and particle size.

According to the Reference [22], it is evident that the quality of deposition is associated with impact velocity, angle and particle size, where the quality of deposition is evaluated by measuring the height of deposition and flattening ratio of the bonded particle. It can be found that different impact velocities, angles and particle sizes result in different flattening ratios, so how to obtain the optimal flattening ratio

by the corresponding parameters (velocity, angle, particle size)? This study proposed a closed loop image aided optimization (CLIAO) method to improve the quality of deposition by obtaining an optimal flattening ratio. In order to form a closed loop optimization, the image processing technique is used to calculate the flattening ratio from the result contours directly. Moreover, several popular optimization methods are employed to obtain the optimal solution which include efficient global optimization (EGO) [23], particle swarm optimization (PSO) [24], differential evolution (DE) algorithm [25]. Furthermore, the back propagation neural network (BPNN) is used to accelerate the optimization process by building a meta-model for the objective function.

The rest of this paper is organized as follows. The theory of the proposed method is introduced in section 2. The results are shown in section 3 and the discussions should be given too. At the last, the conclusion is summarized in section 4.

## 2. Methods

### 2.1. Framework of CLIAO method

The CLIAO method is suggested to obtain the optimal flattening ratio during the cold spray process. The key point is how to calculate the flattening ratio from the result image files instead of data files. Figure2 is the framework of the CLIAO method. It is visible that the CLIAO method contains three loops: the classic optimization loop, the BPNN training loop and the BPNN assisted optimization loop. Obviously, the classic optimization loop is a general process of most methods. Firstly, calculate the value of the objective function, then update the design variables, then calculate the new value of the objective function, then repeat this cycle until satisfying the stopping criterion. MD and image processing technique are used to calculate the value of the objective function in this loop. The second loop, BPNN training loop, is used to build a meta-model of the objective function. Once the BPNN model has been constructed, the value can be evaluated from the BPNN model instead of forward calculation. It can extremely improve the efficiency of classic optimization. The third loop is the BPNN aided optimization loop. Compared with the classic optimization loop, the only difference is the value of objective function should be obtained from the BPNN model directly. More details can be found in the next sections.

### 2.2. MD simulation for cold spray

#### 2.2.1. Basic theories of MD

In the MD simulation, the system is described by the position and momentum of each atom or molecule in the simulation box. The dynamics of atoms obey Newton's law which can be described as the following equation:

$$\begin{aligned} \dot{x}_i &= v_i, \\ m_i \dot{v}_i &= -\nabla_{x_i} V, \end{aligned} \quad (1)$$

where  $m_i$  and  $v_i$  are the mass and velocity of atom  $i$  respectively,  $x_i$  means the position of atom  $i$  and  $V(x_1, x_2, x_3, \dots, x_n)$  denotes the inter-atomic potential. A typical example of the inter-atomic potential is the Embedded Atom Method (EAM) in which an atom should be regarded as the embedded component of a lattice [26]. Specially, the EAM potential can be written as

$$U = \sum_i F_i(\rho_i) + \frac{1}{2} \sum_i \sum_{j \neq i} \phi_{ij}(r_{ij}), \quad (2)$$

$$\rho_i = \sum_{j \neq i} \rho_j(r_{ij}), \quad (3)$$

where  $F_i$  means the embedding energy depended on the electron cloud density  $\rho_i$  around the atom  $i$ . The electron density  $\rho_i$  is associated with all the atoms in the system which can be calculated by Equation(3).

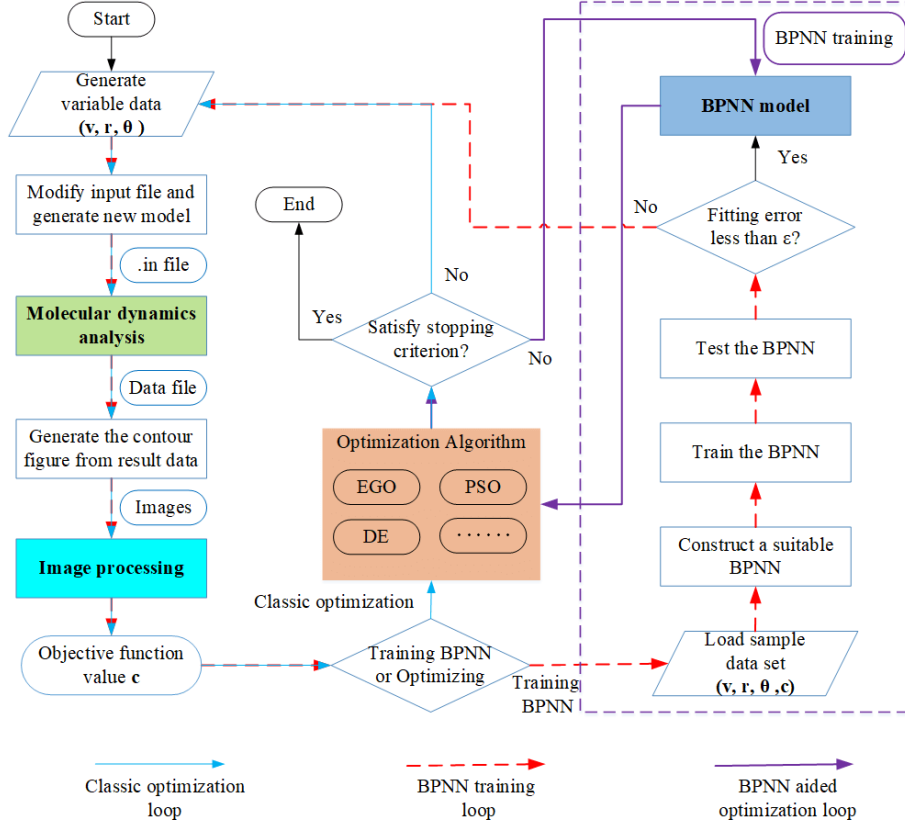


Figure 2: Framework of the CLIAO method

The symbol  $\phi_{ij}$  denotes the pairwise potential, which depends on the relative distance  $r_{ij}$  between atom  $i$  and its neighbor atom  $j$ . Generally, most empirical potentials can be written as

$$V = \sum_i V_i(u_1, u_2, u_3, \dots, u_n), \quad (4)$$

where  $V$  is a function of the energy of each atom ( $V_i$ ), which depends on  $u_i$ , the displacement of atom  $i$  from its reference position  $R_i$  ( $u_i = x_i - R_i$ ). Usually, atoms do not interact directly beyond the cut-off radius  $r_{cut}$ , which implies that

$$\nabla_{x_i} V_i = 0, \text{ if } r_{ij} > r_{cut}. \quad (5)$$

Therefore, the inter-atomic force  $f_i$  on the atom  $i$  can be written as

$$f_i = -\nabla_{u_i} V = \sum_{j \neq i} f_{ij}. \quad (6)$$

There are a series of motion equations needs to solving during the MD simulation, such as Equation(1). Thus, the Velocity-Verlet algorithm is employed as the time integration algorithm to solve the motion equations with a considerable accuracy. More details about the Velocity-Verlet algorithm can be found from the Reference[27].

### 2.2.2. Definition of stress

The definition of stress for an atomic simulation is different from the continuum stress concept. A well-known definition of virial stress suggested by Swenson et al. [28] is used in this study. Atomic scale virial

stresses are equivalent to the continuum Cauchy stresses [29]. The stress contains two parts, potential and kinetic energy parts, which is defined as

$$\sigma_{xy} = \frac{1}{V} \sum_i \left[ \frac{1}{2} \sum_{j=1}^N (r_x^j - r_x^i) f_y^{ij} - m^i v_x^i v_y^i \right], \quad (7)$$

where  $m^i$  means the mass of atom  $i$ , the subscripts  $x$  and  $y$  denote the Cartesian components and  $V$  is the total volume of the system. The superscripts  $i$  and  $j$  are the atom identification number, which mean atom  $i$  and atom  $j$ . The symbols  $r$ ,  $f$  and  $v$  indicate the relative position, inter-atomic force and velocity respectively. Specially, the symbol  $f_y^{ij}$  is the  $y$  direction force on atom  $i$  induced by atom  $j$ ,  $v_x^i$ ,  $r_x^i$  are the velocities and relative position of atom  $i$  along the  $x$  direction. Other symbols are as similar as the above. To roughly calculate the local stress field of the system, the 'atomic stress  $\sigma_{xy}$ ' for each atom in the system is used to plot the stress contours. Here, the 'atomic stress  $\sigma_{xy}$ ' has the unit of stress $\times$ volume. Then the 'Von Mises stress  $\bar{\sigma}$ ' can be calculated by

$$\bar{\sigma} = \frac{1}{\sqrt{2}} \sqrt{(\sigma_x - \sigma_y)^2 + (\sigma_y - \sigma_z)^2 + (\sigma_z - \sigma_x)^2 + 6(\tau_{xy}^2 + \tau_{yz}^2 + \tau_{zx}^2)}, \quad (8)$$

where  $\sigma_x, \sigma_y, \sigma_z$  are the normal stresses and  $\tau_{xy}, \tau_{yz}, \tau_{zx}$  are the tangential stresses.

### 2.2.3. MD model for cold spray

In this study, a classical molecular dynamics code, named Large-scale Atomic/Molecular Massively Parallel Simulator (LAMMPS), is used to simulate the cold spray process [30] and the atomic visualization of the MD simulation results is processed by an open source software termed Open Visualization Tool (OVITO) [31]. This study considers the impact between a nanoparticle and a metal substrate in three-dimension (3D). The material of the simulation is copper (Cu), so both of the nanoparticle and substrate consist of Cu atoms. The substrate is made of about 250,000 atoms and the nanoparticle is made of about 1,000 atoms. Face-centered cubic (FCC) lattice structure is used. Moreover, the schematic of the MD simulation model for the cold spray process is shown in Figure3, where the size of the substrate is  $240\text{\AA} \times 240\text{\AA} \times 50\text{\AA}$  and the radius of nanoparticle is  $15\text{\AA}$ . The constant parameter of FCC lattice structure is  $3.61\text{\AA}$ . More details about the parameters of MD simulation are listed in Table1.

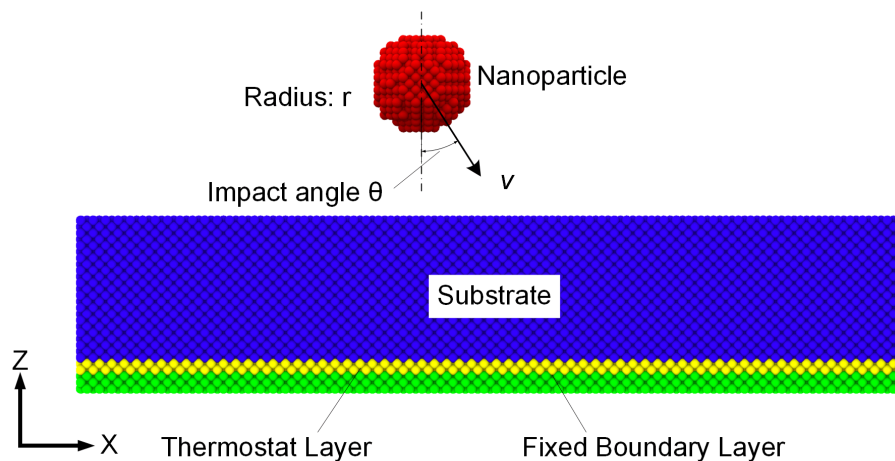


Figure 3: Schematic of MD Simulation Model of Cold spray

Table 1: Parameters of the cold spray MD simulation

Material parameter	Substrate Material	Cu ( $240\text{\AA} \times 240\text{\AA} \times 50\text{\AA}$ ) Approx. 240,000 atoms
	Nanoparticle Material	Cu Sphere ( $Radius 10\text{\AA} - 20\text{\AA}$ ) Approx. 500-2,000 atoms
Simulation parameters	Temperature	298K
	Potential Used	Embedded Atom Method (EAM)
	Initial Stand-off distance	40 $\text{\AA}$
	Impact Velocity	3-12 $\text{\AA}/ps$ (300-1200 $m/s$ )
	Particle Size	10 $\text{\AA} - 20\text{\AA}$
	Angle of Impact	0 $^\circ - 30^\circ$
	Time step	0.001 ps (picoseconds)

### 2.3. Closed loop image aided optimization

The CLIAO method is suggested to obtain the optimal flattening ratio  $\mu$ , where  $\mu$  was defined as a ratio of the maximum diameter of splat (particle after impact) to original diameter of the particle before impact in the Reference[22]. However, it is difficult to define a diameter when the particle impact to the substrate with an angle, because the splat after impact is irregular. Therefore, a generalized flattening ratio  $\mu$  is defined as the ratio of the maximum area ( $S_m$ ) of the splat (particle after impact) to the area of the particle cross section ( $S_i$ ) before impact in this study. Specially, the flattening ratio  $\mu$  is used to measure the quality of deposition during the cold spray process. Consider an example for cold spray as shown in Figure3, where the radius of the particle is  $15\text{\AA}$ , the velocity is  $8\text{\AA}/ps$ , the impact angle is  $0^\circ$ . Then Figure4 shows the snapshots of the MD results before and after impact on top view, where the contour plot is according to the Z-coordinate range from  $0\text{\AA}$  to  $10\text{\AA}$ .

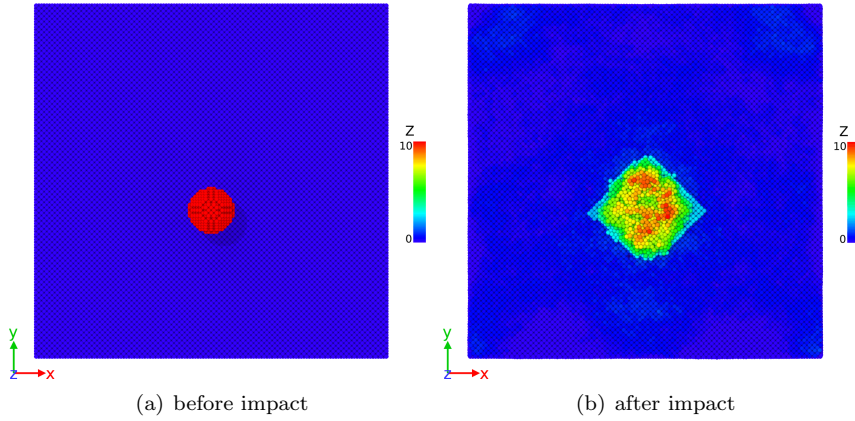


Figure 4: The snapshots of MD computational results on top view

#### 2.3.1. Optimization formulation

As shown in Figure4, once the snapshots of the MD computational results are obtained, then  $S_i$  and  $S_m$  can be obtained from Figure4(a) and 4(b) respectively. Then, the flattening ratio  $\mu$  can be calculated by

$$\mu = S_m/S_i. \quad (9)$$

In order to improve the quality of deposition, the maximum  $\mu$  should be obtained by optimization method. Thus, this optimization problem is formulated as

Minimize:

$$c(v, r, \theta) = \frac{1}{\mu} = \frac{S_i}{S_m}, \quad (10)$$

Subject to:

$$\dot{x}_i = v_i, \quad (11)$$

$$m_i \dot{v}_i = -\nabla_{x_i} V, \quad (12)$$

$$S_i = f(v, r, \theta), \quad (13)$$

$$S_m = f(v, r, \theta), \quad (14)$$

$$300m/s \leq v \leq 1200m/s, \quad (15)$$

$$10\text{\AA} \leq r \leq 20\text{\AA}, \quad (16)$$

$$0^\circ \leq \theta \leq 30^\circ, \quad (17)$$

where  $c(v, r, \theta)$  is the objective function and  $\mu$  means flattening ration mentioned above. The symbols  $v, r, \theta$  denote the velocity, radius, impact angle of particles. Moreover, the cold spray process is simulated by MD, so the objective function also obeys to the Newton's law for MD as shown in equations(11) and (12). It should be noted that the design variables ( $v, r, \theta$ ) are restricted in appropriate intervals in accordance with the practical applications.

### 2.3.2. Image processing technique

As mentioned above, the image processing technique is used to obtain  $S_i$  and  $S_m$  from Figure4, but how to generate the snapshots automatically is the first step need to be completed. In this study, the open source software OVITO is used as the post-processing tool. OVITO is a scientific visualization and analysis software for atomistic and particle simulation data. Specially, OVITO has a powerful Python-based scripting interface which can process and generate various snapshots programmatically. Therefore, a Python script is used to process and generate a series of snapshots such like Figure4. The script can invoke program actions like a human user does in the graphical interface and it can run from the command line without any user interaction, so the snapshots can be generated automatically.

Once the snapshots are generated, the next step is how to extract the splat (particle after impact) from the snapshots. Figure5 shows the process of extracting the splat step by step. It is obvious that the top view snapshot and the substrate background image should be obtained by the Python script firstly. Then make an image difference processing to remove the substrate background from the top view snapshot, so that only the splat (usually located in the central part) will be left in the snapshot. In order to show the result more clearly in the publication, a reversed-phase operation should be applied to the result image which can convert the black background to white. It should be pointed out that this operation is not necessary for the optimization process, is just for the publishing. After that, an image gray processing should be applied to the result image so that the image can be identified clearly by computer. It is worth mentioning that there are some noises in the result image, so a noise filter is used to filter the noises in the last stage. Finally, the splat is separated from the top view snapshot as shown in Figure5, so that  $S_m$  can be calculated by computer easily. Similarly,  $S_i$  can be also obtained by the same way which as shown in Figure6.

### 2.3.3. BPNN assisted optimizations

It is well known that optimization is an iterative process and the MD program need to be evoked again and again, so this is a time-consumed process. Thus, the BPNN is used to accelerate the process by building a mate-model for the objective function. The BPNN is one of the popular artificial neural networks [32]. It's a type of multi-layered feed-forward neural network which can handle nonlinear problem flexibly [33]. The BPNN has been widely used in many fields and algorithms, such as genetic algorithm (GA) [34], PSO [35] and so on.

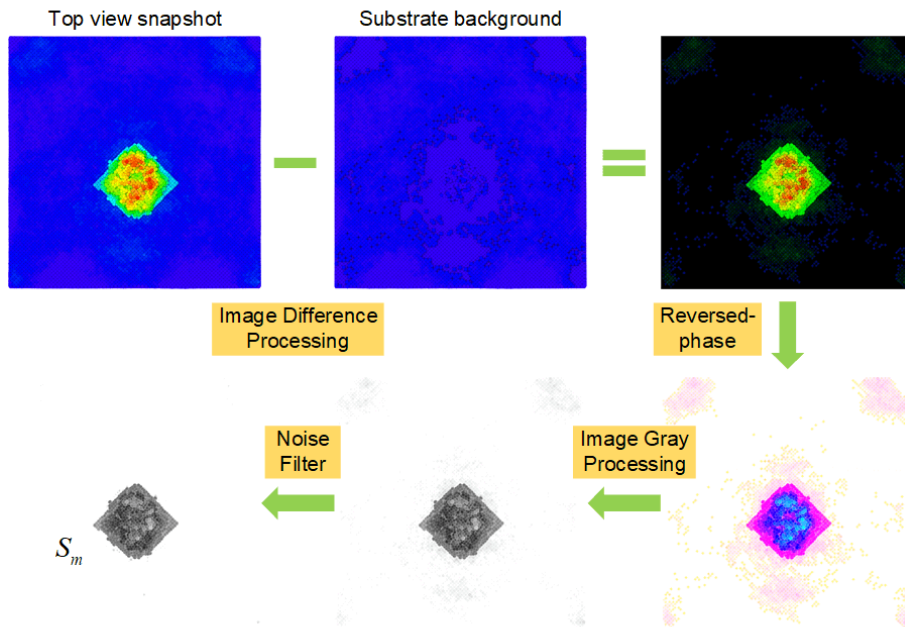


Figure 5: An example of extracting the splat from the snapshot

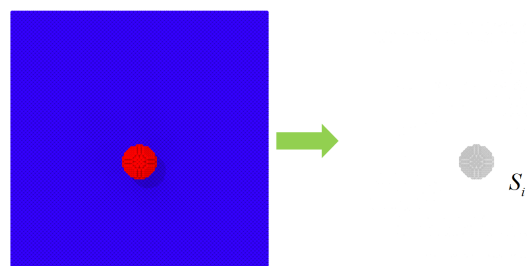


Figure 6: Separating the splat from the snapshot before impact



In this study, the BPNN is used to forecast the value of the objective function, so that the optimal solution can be found more efficiently than the classic optimization loop. Generally, a BPNN is made up of an input layer, an output layer and several hidden layers as shown in Figure7 and the details can be found in the Reference[36]. Furthermore, in order to forecast the value of the objective function, a set of sample data should be used to construct a BPNN, then the BPNN need to be trained, and finally the trained BPNN can be used to forecast the value of objective function.

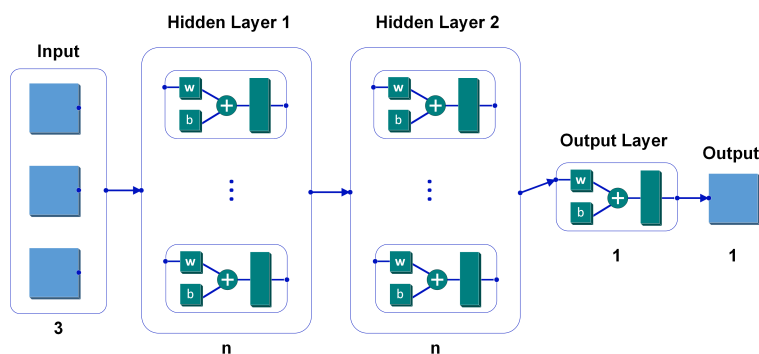


Figure 7: The construction of a BPNN

### 3. Results and discussions

Several popular optimization algorithms including KRG-EGO, PSO, DE are tested and some comparisons are made in this section, where the EGO is started with 20 sample points while PSO and DE is started with 20 particles. All the program is executed under the Linux system and the MD simulation is calculated by parallel LAMMPS with 24 MPI processor. The image processing is realized by Python script and the optimization algorithms are running in Matlab R2017a.

#### 3.1. Results of classic optimization methods

As shown in Figure2, both the classic and the BPNN assisted optimization methods are included and compared in this study. The convergence curves of the objective function in the optimization procedure are shown in Figure8. It can be found that each of these methods can obtain an available solution and behaves great convergent tendency. Specially, EGO is a surrogate optimization method while other two are heuristic algorithms, and it begins with a Kriging surrogate which based on the initial sample set. Then it adds new sample points to the sample set to improve the present optimum and usually the new sample points will be generated one by one according to Kriging surrogate in the single-point EGO algorithm. Thus, the computational cost of EGO is much lower than other two methods. Moreover, it is obvious that the PSO method obtained a better solution than other two methods and converged faster than DE. In a word, the heuristic algorithms (PSO, DE) can obtain a better solution than surrogate optimization methods (EGO) in this problem, but the EGO method is much more efficient than other two methods. The optimal solution of the above three methods is listed in Table2, where  $1\text{\AA}/ps = 100m/s$ . The comparison of the MD simulation results after impact between above three methods is shown in Figure9, where the contour plot is according to the Z-coordinate range from  $0\text{\AA}$  to  $10\text{\AA}$ . Furthermore, the MD simulation snapshots for the optimal solution which obtained by PSO method are shown in Figure10 and the Von Mises stress contour plots are shown in Figure11.

#### 3.2. Results of BPNN assisted optimization methods

As mentioned above, the BPNN is used to accelerate the process of optimization by building a mate-model for the objective function in this study. Thus, 1000 samples are obtained firstly and then used to

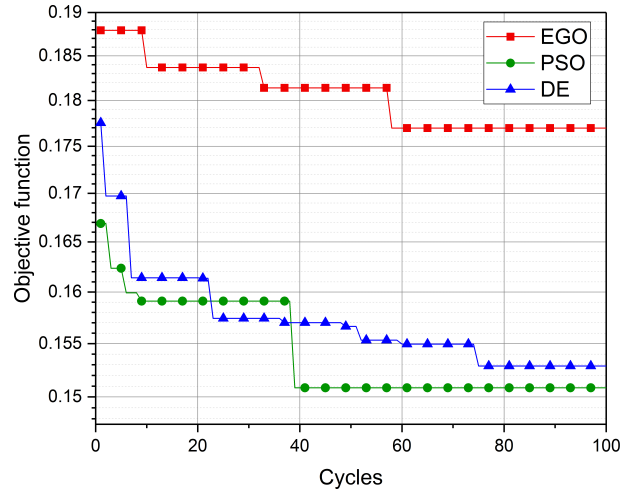


Figure 8: Convergence curve of the objective function in the optimization procedure by different methods

Table 2: Optimal solution of the classic optimization methods

Optimization	Design variables			Objective function
	$v(\text{\AA}/ps)$	$r(\text{\AA})$	$\theta(^{\circ})$	
EGO	12.000	14.736	0.000	0.17697
PSO	12.000	16.145	0.706	0.15084
DE	11.854	16.219	0.000	0.15288

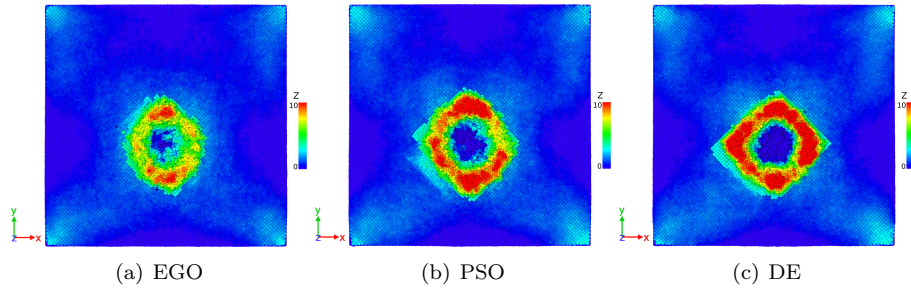


Figure 9: The comparison of the MD simulation results after impact between classic optimizations

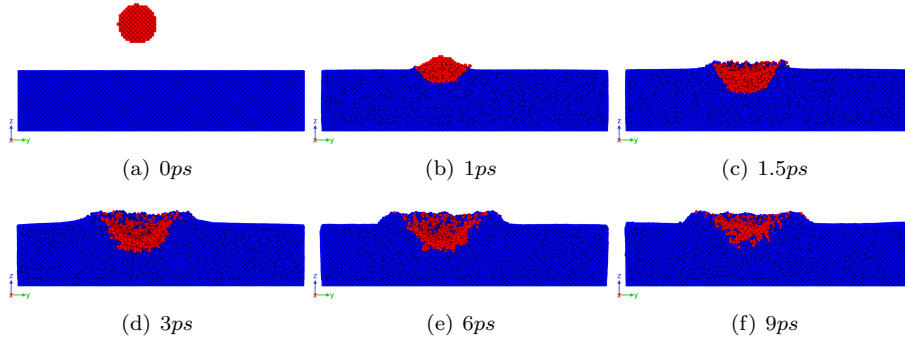


Figure 10: The MD simulation snapshots for the optimal solution (PSO)

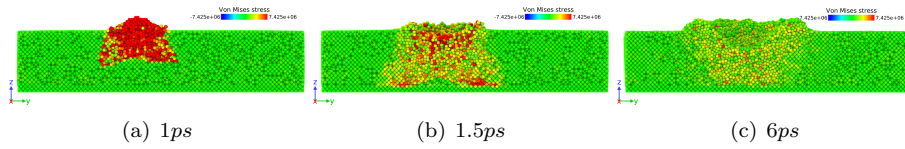


Figure 11: The Von Mises stress contour plots for the optimal solution (PSO)

construct the BPNN model by training, where a triple hidden layer BPNN is used and each hidden layer has 5 nodes. After that, another 1000 samples should be used to test the performance of the BPNN model. The validation performance plot is shown in Figure 12. The regression of the trained BPNN model is shown in Figure 13, and the left is the regression of training samples while the right is the regression of testing samples. Obviously, the performance of the BPNN model is acceptable.

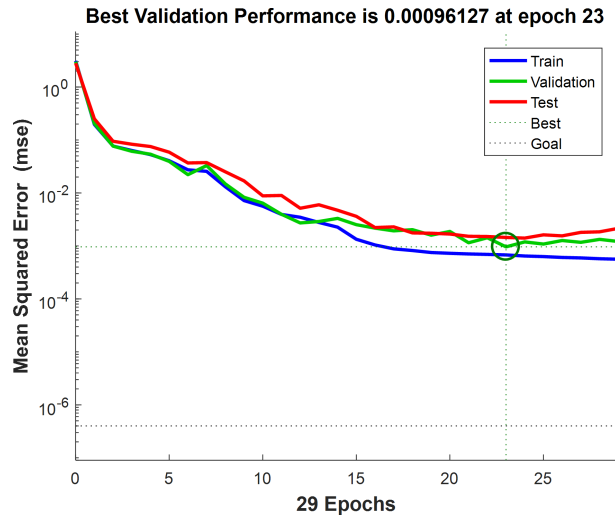


Figure 12: Validation performance of the BPNN model

As for the results of BPNN assisted optimizations, the convergence curves of the objective function in the optimization procedure is shown in Figure14. It can be found that both of these methods are available. Moreover, it is obvious that the BPNN assisted PSO method obtained a better solution than other two methods and converged fast. The optimal solution of the above three methods is listed in Table3, where  $1\text{\AA}/ps = 100m/s$ . The comparison of the MD simulation results after impact between BPNN assisted optimizations are shown in Figure15, where the contour plot is according to the Z-coordinate range from

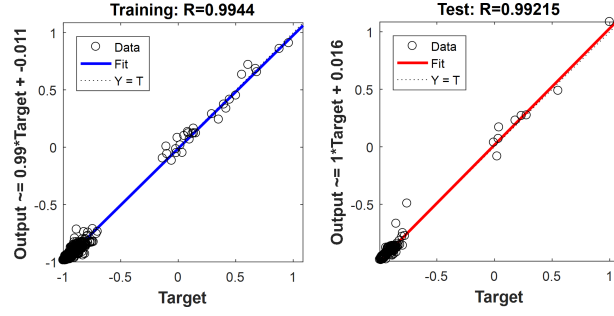


Figure 13: Regression of the BPNN model

0Å to 10Å. Furthermore, the MD simulation snapshots for the optimal solution which obtained by BPNN assisted PSO method are shown in Figure16 and the Von Mises stress contour plots are shown in Figure17.

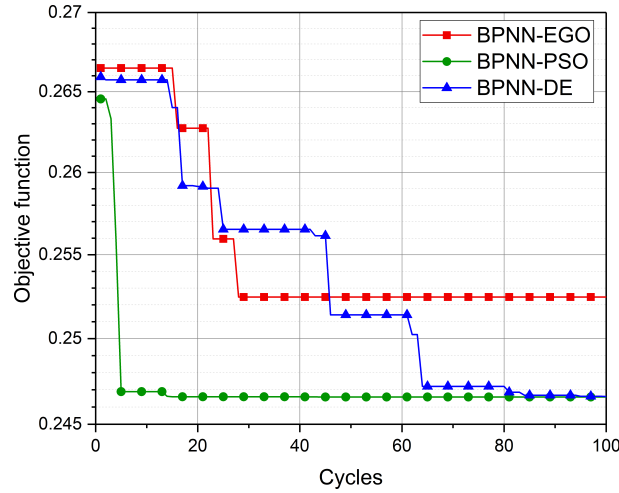


Figure 14: Convergence curve of the objective function in the bpnn assisted optimization procedures

### 3.3. Discussions about classic optimizations and BPNN assisted optimizations

From the above results, it can be found that the performance of BPNN assisted optimizations extremely depends on the accuracy of the BPNN model, so usually the classic optimizations can obtain a better solution than the BPNN assisted optimization methods, but the results of both two kinds of optimization methods are available. Moreover, the computational cost of all the optimization methods is listed as Table4, where  $t_p$  means the computational time for just one sample point by MD simulation. Obviously, EGO is the most efficient method for this problem, but PSO and DE obtain a better solution than EGO. Furthermore, it can be found that the BPNN is not suitable for surrogate optimization (EGO) while it did reduce the computational cost of heuristic algorithms (PSO, DE). Besides, another superiority of the BPNN assisted optimization is the portability, it means the BPNN model can be easily applied to any kind of optimization method once the BPNN model has been constructed. Therefore, which kind of optimization method should be utilized is determined by the trade-off between efficiency and accuracy.

## 4. Conclusion

In this study, a closed loop image aided optimization (CLIAO) method is proposed to improve the quality of deposition during the cold spray process. The main idea of CLIAO method is as follows: firstly, simulate

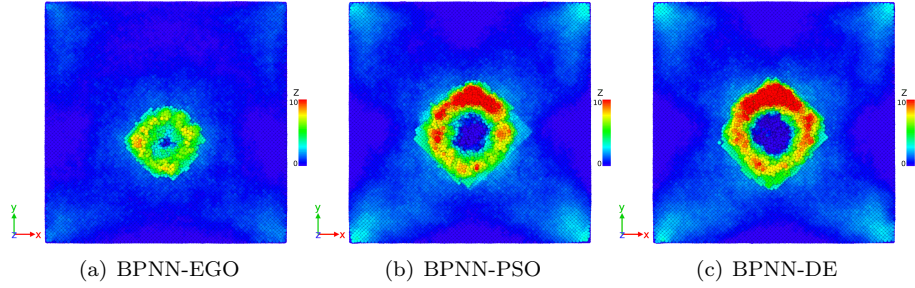


Figure 15: The comparison of the MD simulation results after impact between bpn assisted optimizations

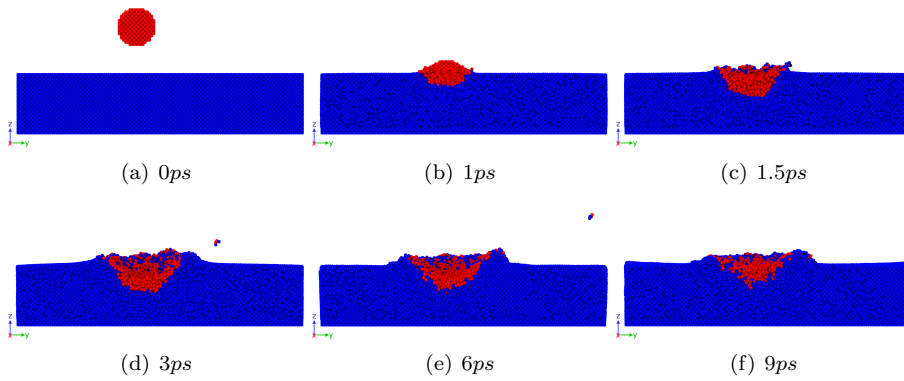


Figure 16: The MD simulation snapshots for the optimal solution (BPNN-PSO)

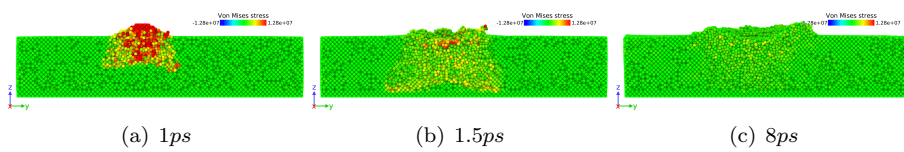


Figure 17: The Von Mises stress contour plots for the optimal solution (BPNN-PSO)

Table 3: Optimal solution of BPNN assisted optimization methods

Optimization	Design variables			Objective function
	$v(\text{\AA}/ps)$	$r(\text{\AA})$	$\theta(^{\circ})$	
BPNN-EGO	12.000	13.1322	0.000	0.25247
BPNN-PSO	12.000	15.917	6.884	0.24658
BPNN-DE	12.000	15.962	6.903	0.24661

Table 4: Computational cost of all the optimization methods

Methods	Modeling cost	Optimization cost	Total cost
EGO	$20t_p$	$100t_p$	$120t_p$
PSO	-	$2000t_p$	$2000t_p$
DE	-	$2000t_p$	$2000t_p$
BPNN-EGO	$1000t_p$	-	$1000t_p$
BPNN-PSO	$1000t_p$	-	$1000t_p$
BPNN-DE	$1000t_p$	-	$1000t_p$

the cold spray process by MD method; then, obtain the value of objective function (flattening ratio) from the result snapshots; finally, find the optimal solution by optimization methods. In order to obtain the flattening ratio from the snapshots directly, the image processing technique is used to generate the required images automatically and calculate the flattening ratio. Moreover, several optimization methods including surrogate optimization (EGO) and heuristic algorithms (PSO, DE) are used to find the optimal solution and the results demonstrated that the PSO method got the best solution while the EGO is the most efficient method. Furthermore, the BPNN is used to accelerate the process of optimization by building a meta-model for objective function and the results shows that the BPNN did improve the efficiency of PSO and DE but it seems not suitable for EGO. In a word, every method has different superiority in efficiency or accuracy, the selection of them should be determined by the trade-off between efficiency and accuracy.

## Acknowledgment

This work is partially supported by Project of the National Key R&D Program of China 2017YFB0203701 and the National Natural Science Foundation of China under the Grant Numbers 11572120. This work is also partially supported by the China Scholarship Council.

## References

## References

- [1] S. Pathak, G. Saha, Development of sustainable cold spray coatings and 3d additive manufacturing components for repair/manufacturing applications: A critical review, *Coatings* 7 (8) (2017) 122. doi:10.3390/coatings7080122.
- [2] A. Alkhimov, V. F. Kosarev, A. Papyrin, A method of cold gas-dynamic spraying, *Doklady Akademii Nauk SSSR* 315 (5) (1990) 1062–1065.
- [3] S. Yin, P. Cavaliere, B. Aldwell, R. Jenkins, H. Liao, W. Li, R. Lupoi, Cold spray additive manufacturing and repair: Fundamentals and applications, *Additive Manufacturing* 21 (2018) 628–650. doi:10.1016/j.addma.2018.04.017.
- [4] H. Assadi, H. Kreye, F. Grtner, T. Klassen, Cold spraying a materials perspective, *Acta Materialia* 116 (2016) 382–407. doi:https://doi.org/10.1016/j.actamat.2016.06.034.

- [5] A. M. Vilardell, N. Cinca, A. Concustell, S. Dosta, I. G. Cano, J. M. Guilemany, Cold spray as an emerging technology for biocompatible and antibacterial coatings: state of art, *Journal of Materials Science* 50 (13) (2015) 4441–4462. doi:10.1007/s10853-015-9013-1.
- [6] A. Papyrin, V. Kosarev, S. Klinkov, A. Alkhimov, V. M. Fomin, *Cold spray technology*, Elsevier, 2006.
- [7] W. Li, K. Yang, S. Yin, X. Yang, Y. Xu, R. Lupoi, Solid-state additive manufacturing and repairing by cold spraying: A review, *Journal of Materials Science & Technology* 34 (3) (2018) 440–457. doi:10.1016/j.jmst.2017.09.015.
- [8] H. Assadi, F. Gärtner, T. Stoltenhoff, H. Kreye, Bonding mechanism in cold gas spraying, *Acta Materialia* 51 (15) (2003) 4379–4394.
- [9] S. Rahmati, A. Ghaei, The use of particle/substrate material models in simulation of cold-gas dynamic-spray process, *Journal of Thermal Spray Technology* 23 (3) (2013) 530–540. doi:10.1007/s11666-013-0051-4.
- [10] M. Yu, W. Y. Li, F. F. Wang, H. L. Liao, Finite element simulation of impacting behavior of particles in cold spraying by eulerian approach, *Journal of Thermal Spray Technology* 21 (3-4) (2011) 745–752. doi:10.1007/s11666-011-9717-y.
- [11] S. Guetta, M. H. Berger, F. Borit, V. Guipont, M. Jeandin, M. Boustie, Y. Ichikawa, K. Sakaguchi, K. Ogawa, Influence of particle velocity on adhesion of cold-sprayed splats, *Journal of Thermal Spray Technology* 18 (3) (2009) 331–342. doi:10.1007/s11666-009-9327-0.
- [12] S. Kumar, G. Bae, C. Lee, Deposition characteristics of copper particles on roughened substrates through kinetic spraying, *Applied Surface Science* 255 (6) (2009) 3472–3479. doi:10.1016/j.apsusc.2008.10.060.
- [13] G. Bae, Y. Xiong, S. Kumar, K. Kang, C. Lee, General aspects of interface bonding in kinetic sprayed coatings, *Acta Materialia* 56 (17) (2008) 4858–4868. doi:10.1016/j.actamat.2008.06.003.
- [14] G. Bae, S. Kumar, S. Yoon, K. Kang, H. Na, H.-J. Kim, C. Lee, Bonding features and associated mechanisms in kinetic sprayed titanium coatings, *Acta Materialia* 57 (19) (2009) 5654–5666. doi:10.1016/j.actamat.2009.07.061.
- [15] S. Kumar, G. Bae, C. Lee, Influence of substrate roughness on bonding mechanism in cold spray, *Surface and Coatings Technology* 304 (2016) 592–605. doi:10.1016/j.surfcoat.2016.07.082.
- [16] M. Grujicic, J. R. Saylor, D. E. Beasley, W. S. DeRosset, D. Helfritsch, Computational analysis of the interfacial bonding between feed-powder particles and the substrate in the cold-gas dynamic-spray process, *Applied Surface Science* 219 (3-4) (2003) 211–227. doi:10.1016/s0169-4332(03)00643-3.
- [17] A. Manap, O. Nooririnah, H. Misran, T. Okabe, K. Ogawa, Experimental and sph study of cold spray impact between similar and dissimilar metals, *Surface Engineering* 30 (5) (2014) 335–341. doi:10.1179/1743294413y.0000000237.
- [18] W. Y. Li, S. Yin, X. F. Wang, Numerical investigations of the effect of oblique impact on particle deformation in cold spraying by the sph method, *Applied Surface Science* 256 (12) (2010) 3725–3734. doi:10.1016/j.apsusc.2010.01.014.
- [19] B. Daneshian, H. Assadi, Impact behavior of intrinsically brittle nanoparticles: A molecular dynamics perspective, *Journal of Thermal Spray Technology* 23 (3) (2013) 541–550. doi:10.1007/s11666-013-0019-4.
- [20] S. Goel, N. H. Faisal, V. Ratia, A. Agrawal, A. Stukowski, Atomistic investigation on the structure-property relationship during thermal spray nanoparticle impact, *Computational Materials Science* 84 (2014) 163–174. doi:10.1016/j.commatsci.2013.12.011.
- [21] H. L. Yao, G. J. Yang, C. J. Li, Md simulation on collision behavior between nano-scale tio(2) particles during vacuum cold spraying, *J Nanosci Nanotechnol* 18 (4) (2018) 2657–2664. doi:10.1166/jnn.2018.14284.
- [22] A. Joshi, S. James, Molecular dynamics simulation study of cold spray process, *Journal of Manufacturing Processes* 33 (2018) 136–143. doi:10.1016/j.jmapro.2018.05.005.
- [23] D. R. Jones, M. Schonlau, W. J. Welch, Efficient global optimization of expensive black-box functions, *Journal of Global optimization* 13 (4) (1998) 455–492.
- [24] J. Kennedy, Particle swarm optimization, in: *Encyclopedia of machine learning*, Springer, 2011, pp. 760–766.
- [25] R. Storn, K. Price, Differential evolution—a simple and efficient heuristic for global optimization over continuous spaces, *Journal of global optimization* 11 (4) (1997) 341–359.
- [26] M. S. Daw, M. I. Baskes, Semiempirical, quantum mechanical calculation of hydrogen embrittlement in metals, *Physical review letters* 50 (17) (1983) 1285.
- [27] I. Omelyan, I. Mryglod, R. Folk, Optimized verlet-like algorithms for molecular dynamics simulations, *Physical Review E* 65 (5) (2002) 056706.
- [28] R. J. Swenson, Comments on virial theorems for bounded systems, *American Journal of Physics* 51 (10) (1983) 940–942.
- [29] A. K. Subramaniyan, C. Sun, Continuum interpretation of virial stress in molecular simulations, *International Journal of Solids and Structures* 45 (14-15) (2008) 4340–4346.
- [30] S. Plimpton, Fast parallel algorithms for short-range molecular dynamics, *Journal of computational physics* 117 (1) (1995) 1–19.
- [31] A. Stukowski, Visualization and analysis of atomistic simulation data with ovito: the open visualization tool, *Modelling and Simulation in Materials Science and Engineering* 18 (1) (2010) 015012.
- [32] A. T. Goh, Back-propagation neural networks for modeling complex systems, *Artificial Intelligence in Engineering* 9 (3) (1995) 143–151.
- [33] G. Zhang, B. E. Patuwo, M. Y. Hu, Forecasting with artificial neural networks: The state of the art, *International journal of forecasting* 14 (1) (1998) 35–62.
- [34] R. Irani, R. Nasimi, Evolving neural network using real coded genetic algorithm for permeability estimation of the reservoir, *Expert Systems with Applications* 38 (8) (2011) 9862–9866.
- [35] J.-R. Zhang, J. Zhang, T.-M. Lok, M. R. Lyu, A hybrid particle swarm optimization–back-propagation algorithm for feedforward neural network training, *Applied mathematics and computation* 185 (2) (2007) 1026–1037.
- [36] L. Zhang, G. Subbarayan, An evaluation of back-propagation neural networks for the optimal design of structural systems: Part ii. numerical evaluation, *Computer Methods in Applied Mechanics and Engineering* 191 (25-26) (2002) 2887–2904.